Surface Structure of $V_2O_3(0001)$ Revisited

Felix E. Feiten,[1] Jan Seifert,[1,2] Joachim Paier,[3,†] Helmut Kuhlenbeck,[1,*] Helmut Winter,[2] Joachim Sauer,[3] and Hans-Joachim Freund[1]

[1]*Fritz-Haber-Institut der Max-Planck-Gesellschaft, Faradayweg 4-6, 14195 Berlin, Germany*
[2]*Humboldt-Universität zu Berlin, Institut für Physik, Newtonstrasse 15, 12489 Berlin, Germany*
[3]*Humboldt-Universität zu Berlin, Institut für Chemie, Unter den Linden 6, 10099 Berlin, Germany*

(Received 20 January 2015; published 26 May 2015)

In a recent paper [A. J. Window *et al.*, Phys. Rev. Lett. 107, 016105 (2011)], it was proposed that $V_2O_3(0001)$ is terminated by the so-called O_3 termination, a reconstruction with a terminating distorted hexagonal oxygen layer. We show that the surface is terminated by vanadyl (V=O) groups instead. This conclusion is based on quantitative low-energy electron diffraction combined with scanning tunneling microscopy, fast atom scattering, and density functional theory employing the Heyd-Scuseria-Ernzerhof functional. New insights into the subsurface sensitivity of ion beam triangulation show that results previously interpreted in favor of the O_3 termination are reconcilable with vanadyl termination as well.

DOI: 10.1103/PhysRevLett.114.216101 PACS numbers: 68.35.B-, 61.05.jh, 68.47.Gh

Vanadium oxides find significant interest in basic research and are of technological importance because of their metal to insulator transitions and applications in oxygen transfer catalysis [1–5]. The surface termination is of decisive relevance for both classes of applications—this is obvious for the area of catalysis, but the influence on phase transitions, at least in near-surface layers, has also been shown [6]. For $V_2O_3(0001)$, a number of studies have been published, but there is still an ongoing debate about its termination [7–14].

For almost a decade, the $V_2O_3(0001)$ surface prepared under ultrahigh vacuum (UHV) conditions was assumed to be vanadyl terminated. This conclusion was based mainly on the presence of an intense vanadyl signal in vibrational spectra [7,8], but scanning tunneling microscopy (STM), X-ray photoelectron spectroscopy, and near edge X-ray absorption fine structure data also supported this view [7,8,15]. However, recent studies employing ion scattering and density functional theory (DFT) strongly favor the O_3 termination [9–11].

Motivated by this controversy, we have performed an extensive quantitative surface structure determination employing low-energy electron diffraction (LEED) and *I-V* LEED combined with STM, as well as fast atom scattering and DFT. Furthermore, we reinterpret the results of a previous ion scattering study [10].

The hexagonal bulk unit cell of V_2O_3 gives rise to three different possible terminations when cutting parallel to the 0001 plane: metal terminations with two vanadium atoms [double metal (DM)] ($\cdots O_3{-}V_2{-}O_3{-}V_2$) and one vanadium atom [single metal (SM)] ($\cdots O_3{-}V_2{-}O_3{-}V$) in the surface unit cell, respectively, and an oxygen termination ($\cdots O_3{-}V_2{-}O_3$). DFT calculations indicate that several reconstructions are energetically favorable over the bulk terminations [12,13]. At low oxygen chemical potential a vanadyl-covered surface ($\cdots O_3{-}V_2{-}O_3{-}V{=}O$) is thermodynamically stable, while at higher oxygen chemical potential incomplete V=O terminations form, with ordered superstructures at 2/3 and 1/3 of the full V=O coverage and finally an O_3 termination completely devoid of V=O groups. Compared to the bulklike, oxygen-terminated surface, this O_3 termination is reconstructed with each second V atom from the second layer moved up into the first layer ($\cdots O_3{-}V{-}O_3{-}V_3{-}O_3$) as shown in Fig. 1.

About 100 Å thick $V_2O_3(0001)$ films were prepared on Au(111) by deposition of vanadium from an *e*-beam evaporator with a rate of ~0.7 Å/ min in an O_2 ambience, followed by annealing in oxygen and finally in UHV for a short time. Some films were afterwards oxidized by annealing at elevated oxygen pressures. While films deposited at 1×10^{-7} mbar$< p(O_2) < 1 \times 10^{-6}$ mbar show a (1×1) LEED pattern, a $(\sqrt{3} \times \sqrt{3})R30°$ superstructure appears after exposure to higher O_2 pressures. This is the first clear evidence that none of the prepared layers was O_3

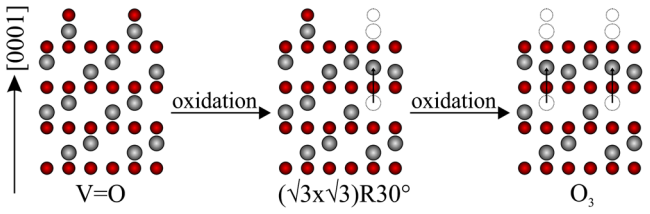

FIG. 1 (color online). Structural model (V gray and O red) of surface terminations predicted by DFT.

*Corresponding author.
kuhlenbeck@fhi-berlin.mpg.de
†To whom all correspondence regarding the density functional computations should be addressed.
joachim.paier@chemie.hu-berlin.de

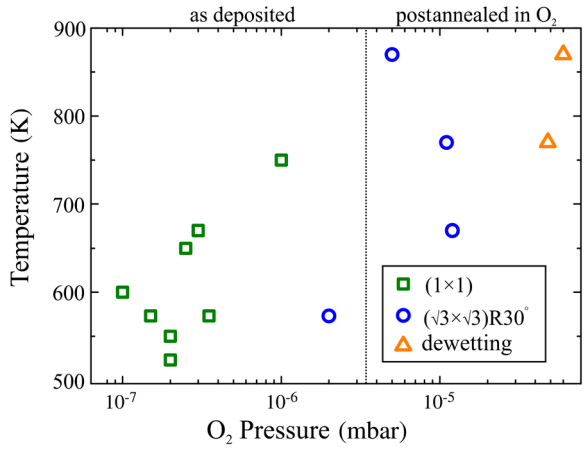

FIG. 2 (color online). Experimentally observed surface phases as a function of the preparation conditions.

terminated, since the oxygen content in the O_3 structure is higher than in the $(\sqrt{3} \times \sqrt{3})R30°$ phase. At even higher oxygen pressure, the film disappeared, probably through formation of V_2O_5, which sublimates at above ~800 K [16]. An overview of the observed phases is shown in Fig. 2.

While the $(\sqrt{3} \times \sqrt{3})R30°$ termination can easily be identified by LEED, both the V=O-covered surface and the O_3 termination exhibit identical reflex patterns. Thus, *I-V* LEED analysis was used to differentiate between these structures and to determine the positions of the atoms at the surface. For this study, the intensities of 32 diffraction spots were recorded. Averaging over symmetry equivalent spots and different domains yielded eight different beams over a combined energy range of 1819 eV. Beam damage was minimized by use of a LEED system with a microchannel plate detector, reducing electron currents to the surface to less than 10 nA. *I-V* curves were calculated with a modified version of the SATLEED package of Barbieri and van Hove [17]. The Pendry *R* factor [18] was used to quantify the agreement between theory and experiment—a smaller *R* factor means better agreement. The structures were refined by minimization of the *R* factor using a covariance matrix adaptation evolution strategy as implemented in the SHARK library [19]. Depending on the structural model, 15–17 atomic coordinates and three to five Debye temperatures as well as the imaginary and real parts of the inner potential and a linear background of the experimental data were selected as refinement parameters.

A total of 14 different structures with varying interlayer distances (five SM, five V=O, two DM, and two O_3 [11,12,20,21]) were selected as start structures for the refinement. Out of all models, coordinates published by Czekaj, Hermann, and Witko [20] for a V=O-terminated surface led to the smallest *R* factor after refinement ($R = 0.12$) [22]. In contrast, the smallest *R* factor for the O_3 termination is 0.36. The corresponding *I-V* curves shown in Fig. 3 visualize the good agreement between the

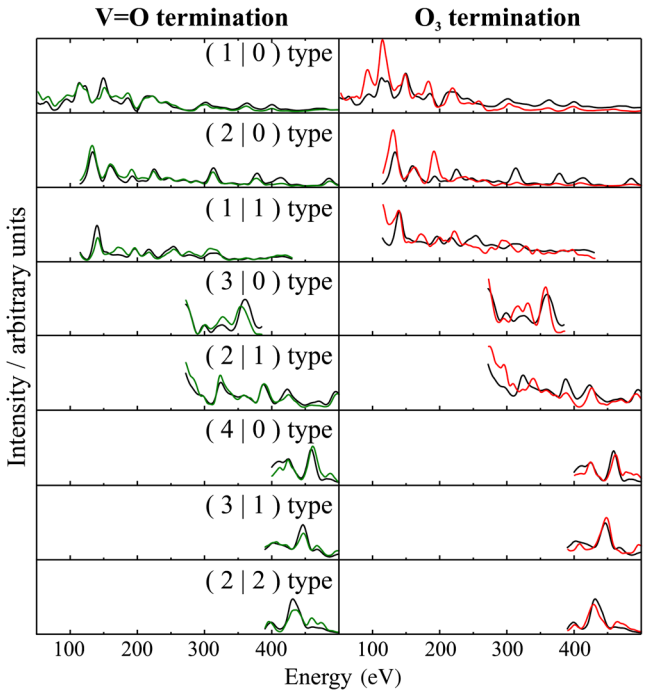

FIG. 3 (color online). Calculated *I-V* LEED curves (green and red) and experimental data (black) for the eight symmetry inequivalent beams.

V=O simulation and the experiment, while there are clear deviations from the experimental curves for the best-fit simulation of the O_3 termination.

STM images obtained for the (1×1) phase always show a hexagonal lattice (Fig. 4). This type of STM image is consistent with Tersoff-Hamann simulations for a fully vanadyl-covered surface, while the triangular features characteristic of an O_3 termination [11] or a bulklike oxygen termination [23] were never seen. Figure 4(a) shows an image taken directly after recording the *I-V* curves shown in Fig. 3. The bright triangular features are attributed to a slight reduction of the surface. In Fig. 4(b), a slightly oxidized surface is imaged. Herein dark depressions correspond to missing V=O groups [8].

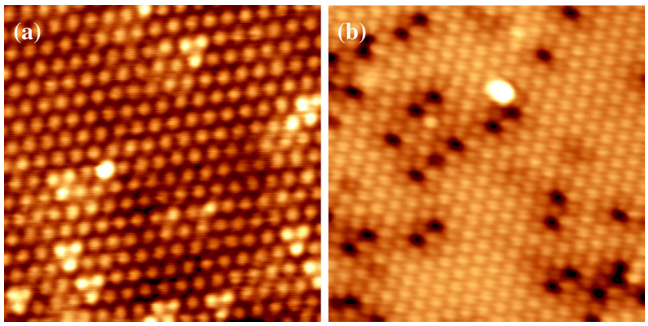

FIG. 4 (color online). Atomically resolved STM images of the $V_2O_3(0001)$ surface. (a) Slightly reduced layer; (b) slightly overoxidized layer. 10×10 nm^2, 2 V, and 0.1 nA.

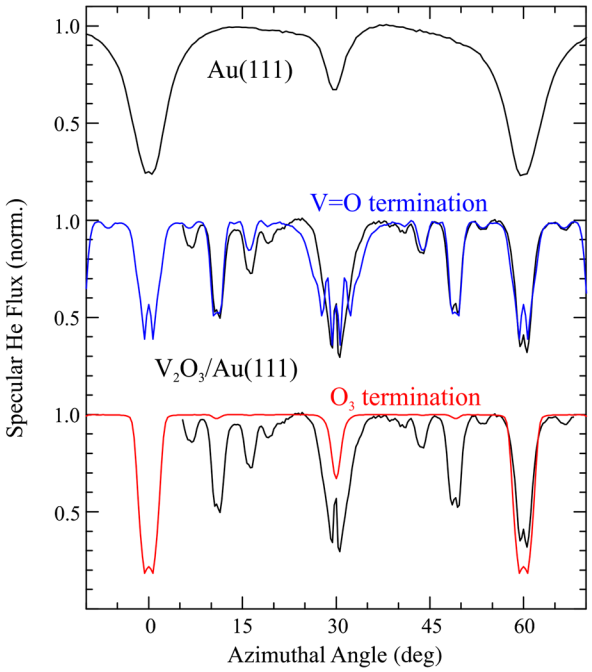

FIG. 5 (color online). Intensity of specularly reflected 2 keV He atoms (black curve) from Au(111) and a $V_2O_3(0001)$ thin film as a function of the azimuthal angle as well as simulations for the vanadyl (blue curve) and O_3 termination (red curve) of $V_2O_3(0001)$.

Further evidence is provided by grazing angle scattering of 2 keV He atoms. In this experiment the flux of specularly reflected He atoms was recorded as a function of the azimuthal rotation of the sample for a polar incidence angle of 1° with respect to the surface plane. Incidence along a principal axis, i.e., for scattering along a line of densely packed atoms, leads to a broadening of the angular distribution and thus to a reduction of the flux in the specular direction. In Fig. 5, this flux is plotted for Au(111) (upper panel) and a $V_2O_3(0001)$ film (lower panels). The data are compared with simulations based on classical trajectories using a superposition of atomic pair potentials as described elsewhere [24]. For the vanadyl termination (blue curve) good overall agreement is observed, whereas the close packing of surface oxygen atoms in the O_3 model (red curve) leads to narrow axial channels with little lateral deflection of scattered projectiles for most directions. The simulated curve deviates significantly from the experimental one.

This finding seems to be in conflict with a recent ion beam triangulation study [10] which favored the O_3 termination. In this study, electron emission following the grazing scattering from the surface of 25 keV H atoms was recorded as a function of the azimuthal surface orientation. For close-packed crystal surfaces, thin films, and adsorbate systems, a high surface sensitivity of ion beam triangulation has been demonstrated [25,26]. However, for one monolayer of the amino acid alanine on Cu(110) [24], a curve similar to that for the clean substrate was obtained, whereas from triangulation, based on the specular flux of 2 keV He atoms, information on the position of the topmost methyl groups is obtained. A similar issue may also be in effect for the $V_2O_3(0001)$ surface, where the relatively sparsely distributed vanadyl groups may affect the emission of electrons to a lesser extent than previously assumed.

Since DFT has been invoked to support the O_3 surface termination [9], we examine the sensitivity of DFT results with respect to the choice of the exchange-correlation functional, specifically with respect to Fock exchange. The screened hybrid functional after Heyd, Scuseria, and Ernzerhof (HSE) [27] with a range-separation parameter of 0.207 $Å^{-1}$ was used. Spin polarization was not included, because at ambient temperature V_2O_3 is a nonmagnetic metal crystallizing in the rhombohedral corundum structure. Our spin-unpolarized DFT calculations use the VASP code and employ projector-augmented plane waves (PAWs) up to a kinetic energy of 600 eV [28–30]. The electron-ion interaction was described by using PAW pseudopotentials with $3p^6 3d^3 4s^2$ and $2s^2 2p^4$ as valence electrons for V and O, respectively. Symmetric slab models of the primitive surface unit cell with a lattice constant of 4.933 Å (HSE equilibrium lattice constant) and 30 atomic layers were used, and a vacuum layer of approximately 10 Å was employed to separate periodic images of the slabs. To model the bulk, two innermost V atoms and one neighboring O trilayer per V were kept frozen at bulk positions. Forces acting on the atoms in the remaining 26 layers were relaxed to better than 0.05 eV/Å. To sample the surface Brillouin zone, Γ-centered Monkhorst-Pack meshes using $(2 \times 2)k$ points were used. Energies obtained by using a $(4 \times 4)k$ mesh (single points) consistently shifted the intercepts of the linear equations for surface energies by less than 6 meV/$Å^2$; thus, the results did not change qualitatively.

Schwingenschlögl and co-workers found that lowering the amount of Fock exchange (FX) from 25% to 10% in the HSE hybrid functional results in a more balanced description of the VO_2 bulk phases [31]. However, we found that HSE using the "as defined" amount of FX of 25% outperforms the Perdew-Burke-Ernzerhof (PBE) [32] functional, which is based on the generalized-gradient approximation (GGA) and does not include Fock exchange. HSE heats of formation for V_2O_3, V_2O_4, and V_2O_5 agree better with observed values than PBE results. Also, the oxidation of V_2O_3 to V_2O_4 is better described by using the HSE functional [33]. We do not claim that a simple hybrid functional like HSE consistently captures the complex physics of V_2O_3 mostly driven by Coulomb correlation effects, but based on the aforementioned thermochemical results we believe that HSE surface stabilities are more reliable than results obtained by using the PBE or the closely related Perdew-Wang 1991 GGA-type functionals used in earlier work [12]. Recent HSE results by Rubio

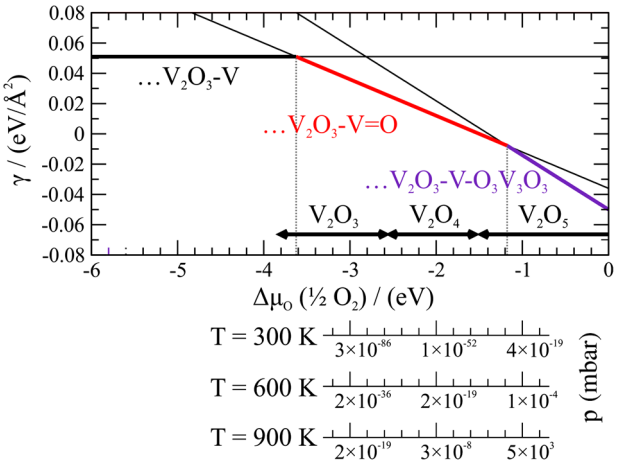

FIG. 6 (color online). Surface energy γ as a function of the chemical potential $\Delta\mu_O$ for different terminations of the $V_2O_3(0001)$ surface. At the bottom, the chemical potential scale is transformed into O_2 pressure scales (mbar) for different temperatures. The stability ranges of the bulk phases are indicated by the horizontal black arrows.

and co-workers [34], which describe the metal-insulator transition in paramagnetic V_2O_3 correctly, provide further support for our findings.

When adding some FX to the GGA-based functional, the highest oxygen chemical potential, for which V=O termination is calculated to be thermodynamically favorable, increases from −2.3 (which is exactly the same as the PBE functional, i.e., no FX) through −1.9 (HSE with 10% FX) to −1.2 eV (HSE with 25% FX).

The phase diagram calculated with HSE is shown in Fig. 6. Phase diagrams for pure GGA as well as for 10% FX are provided in Supplemental Material [35]. The oxygen chemical potential $\Delta\mu_O(\frac{1}{2}O_2)$ uses half of the total energy of the O_2 molecule as a reference. Tabulated values for the enthalpy H and entropy S at the temperature T were used [36]. Further details on the pressure and temperature dependence of $\Delta\mu_O$ can be found in Refs. [37,38]. Black arrows at the bottom refer to the stable bulk phases at the respective chemical potentials, while the bold lines above indicate the expected surface terminations. Figure 6 shows that the V=O termination is predicted to be thermodynamically stable over a wide range of oxygen chemical potentials. As also shown previously [12], the V=O termination cannot be reduced by heating in UHV, since the required potential is too negative to be realized experimentally. While conditions that would favor the O_3 termination are experimentally accessible, the stable bulk phase expected under these conditions is already V_2O_5, in agreement with the findings summarized in Fig. 2, which indicate that the oxide layer sublimates. We note that, according to the DFT calculations, V_2O_3 is not the equilibrium bulk phase for all preparation conditions employed in this study. This is a hint that the formation of higher oxides is just prevented by kinetic limitations.

In conclusion, we have shown that the $V_2O_3(0001)$ surface, prepared under standard UHV conditions, is terminated by vanadyl groups. *I-V* LEED measurements and fast atom scattering are clearly in favor of this termination, like the STM results. Recent ion beam triangulation results are also reconcilable with a vanadyl-terminated surface.

In a recent study, Window *et al.* [9] proposed that the surface might be terminated by an equilibrium mixture of O_3 and V=O areas with a small V=O contribution in order to explain the presence of the V=O stretching vibration in vibrational spectra. Neither our STM studies, which always show the presence of a single phase for well-prepared layers, nor our DFT calculations, which predict the vanadyl termination to be stable under the relevant conditions, support this conclusion. DFT shows that the O_3 termination is drastically destabilized. Even if one assumes an error of several hundred meV in the chemical potential of oxygen, which corresponds to several orders of magnitude of an error in the pressure, a phase equilibrium between V=O and O_3 with a noticeable contribution of the O_3 phase cannot be reached. This is in marked contrast to previous DFT studies [12,13] and can be attributed to the higher accuracy of the HSE hybrid functional as shown by, compared with experiment, improved formation enthalpies of bulk V_xO_y phases [33].

This work was supported by the Deutsche Forschungsgemeinschaft (DFG) through their collaborative research center 546, "Transition Metal Oxide Aggregates." We also acknowledge support from the Fonds der Chemischen Industrie, the North-German Supercomputing Alliance in Berlin and Hannover (HLRN; grants for computing time), and thank Horst Niehus for helpful discussions.

*Corresponding author.
kuhlenbeck@fhi-berlin.mpg.de
†To whom all correspondence regarding the density functional computations should be addressed.
joachim.paier@chemie.hu-berlin.de

[1] K. Held, G. Keller, V. Eyert, D. Vollhardt, and V. I. Anisimov, Phys. Rev. Lett. **86**, 5345 (2001).
[2] S. Surnev, M. Ramsey, and F. Netzer, Prog. Surf. Sci. **73**, 117 (2003).
[3] G. Deo and I. E. Wachs, J. Catal. **146**, 323 (1994).
[4] G. C. Bond and S. F. Tahir, Appl. Catal. **71**, 1 (1991).
[5] D. Göbke, Y. Romanyshyn, S. Guimond, J. M. Sturm, H. Kuhlenbeck, J. Döbler, U. Reinhardt, M. V. Ganduglia-Pirovano, J. Sauer, and H.-J. Freund, Angew. Chem., Int. Ed. Engl. **48**, 3695 (2009).
[6] F. Pfuner, J. Schoiswohl, M. Sock, S. Surnev, M. G. Ramsey, and F. P. Netzer, J. Phys. Condens. Matter **17**, 4035 (2005).
[7] A.-C. Dupuis, M. Abu-Haija, B. Richter, H. Kuhlenbeck, and H.-J. Freund, Surf. Sci. **539**, 99 (2003).

[8] J. Schoiswohl, M. Sock, S. Surnev, M. Ramsey, F. Netzer, G. Kresse, and J. Andersen, Surf. Sci. **555**, 101 (2004).
[9] A. J. Window, A. Hentz, D. C. Sheppard, G. S. Parkinson, H. Niehus, D. Ahlbehrendt, T. C. Q. Noakes, P. Bailey, and D. P. Woodruff, Phys. Rev. Lett. **107**, 016105 (2011).
[10] J. Seifert, E. Meyer, H. Winter, and H. Kuhlenbeck, Surf. Sci. **606**, L41 (2012).
[11] A. J. Window, A. Hentz, D. C. Sheppard, G. S. Parkinson, D. P. Woodruff, W. Unterberger, T. C. Q. Noakes, P. Bailey, M. Ganduglia-Pirovano, and J. Sauer, Surf. Sci. **606**, 1716 (2012).
[12] G. Kresse, S. Surnev, J. Schoiswohl, and F. P. Netzer, Surf. Sci. **555**, 118 (2004).
[13] T. K. Todorova, M. V. Ganduglia-Pirovano, and J. Sauer, J. Phys. Chem. B **109**, 23523 (2005).
[14] I. Czekaj, K. Hermann, and M. Witko, Surf. Sci. **545**, 85 (2003).
[15] C. Kolczewski, K. Hermann, S. Guimond, H. Kuhlenbeck, and H.-J. Freund, Surf. Sci. **601**, 5394 (2007).
[16] S. Guimond, J. M. Sturm, D. Göbke, Y. Romanyshyn, M. Naschitzki, H. Kuhlenbeck, and H.-J. Freund, J. Phys. Chem. C **112**, 11835 (2008).
[17] A. Barbieri and M. van Hove, private communication, http://www.icts.hkbu.edu.hk/vanhove/.
[18] J. B. Pendry, J. Phys. C Solid State Phys. **13**, 937 (1980).
[19] C. Igel, V. Heidrich-Meisner, and T. Glasmachers, J. Mach. Learn. Res. **9**, 993 (2008).
[20] I. Czekaj, K. Hermann, and M. Witko, Surf. Sci. **525**, 33 (2003).
[21] E. A. Kröger, D. I. Sayago, F. Allegretti, M. J. Knight, M. Polcik, W. Unterberger, T. J. Lerotholi, K. A. Hogan, C. L. A. Lamont, and D. P. Woodruff, Surf. Sci. **601**, 3350 (2007).
[22] See Fig. S1 in Supplemental Material at http://link.aps.org/supplemental/10.1103/PhysRevLett.114.216101 for structural data of the best-fit models.
[23] S. Surnev, G. Kresse, M. Sock, M. G. Ramsey, and F. P. Netzer, Surf. Sci. **495**, 91 (2001).
[24] J. Seifert, M. Busch, E. Meyer, and H. Winter, Phys. Rev. B **89**, 075404 (2014).
[25] T. Bernhard, J. Seifert, and H. Winter, J. Phys. Condens. Matter **21**, 134001 (2009).
[26] J. Seifert and H. Winter, Nucl. Instrum. Methods Phys. Res., Sect. B **315**, 9 (2013).
[27] J. Heyd, G. E. Scuseria, and M. Ernzerhof, J. Chem. Phys. **118**, 8207 (2003); **124**, 219906 (2006).
[28] G. Kresse and J. Furthmüller, Phys. Rev. B **54**, 11169 (1996).
[29] G. Kresse and D. Joubert, Phys. Rev. B **59**, 1758 (1999).
[30] P. E. Blöchl, Phys. Rev. B **50**, 17953 (1994).
[31] H. Wang, T. A. Mellan, R. Grau-Crespo, and U. Schwingenschlögl, Chem. Phys. Lett. **608**, 126 (2014).
[32] J. P. Perdew, K. Burke, and M. Ernzerhof, Phys. Rev. Lett. **77**, 3865 (1996).
[33] See Tables S3 and S4 in Supplemental Material at http://link.aps.org/supplemental/10.1103/PhysRevLett.114.216101 for tables showing bulk heats of formation and heats of reactions.
[34] F. Iori, M. Gatti, and A. Rubio, Phys. Rev. B **85**, 115129 (2012).
[35] See Fig. S2 in Supplemental Material at http://link.aps.org/supplemental/10.1103/PhysRevLett.114.216101 for phase diagrams of pure GGA and 10% FX.
[36] *CRC Handbook of Chemistry and Physics*, edited by D. R. Lide and H. P. Frederiske, 76th ed. (CRC Press, Boca Raton, FL, 1995).
[37] K. Reuter and M. Scheffler, Phys. Rev. B **65**, 035406 (2001).
[38] M. V. Ganduglia-Pirovano and J. Sauer, Phys. Rev. B **70**, 045422 (2004).